Aalborg Universitet

AALBORG UNIVERSITY

DENMARK

A new approach of kinematic geometry for error identification and compensation of industrial robots

Wang, Zhi; Dong, Huimin; Bai, Shaoping; Wang, Delun

A new approach of kinematic geometry for error identification and compensation of industrial robots

Zhi Wang[1] , Huimin Dong[1], Shaoping Bai[1,2] and Delun Wang[1]

Abstract

A new approach for kinematic calibration of industrial robots, including the kinematic pair errors and the link errors, is developed in this paper based on the kinematic invariants. In most methods of kinematic calibration, the geometric errors of the robots are considered in forms of variations of the link parameters, while the kinematic pairs are assumed ideal. Due to the errors of mating surfaces in kinematic pairs, the fixed and moving axes of revolute pairs, or the fixed and moving guidelines of prismatic pairs, are separated, which can be concisely identified as the kinematic pair errors and the link errors by means of the kinematic pair errors model, including the self-adaption fitting of a ruled surface, or the spherical image curve fitting and the striction curve fitting. The approach is applied to the kinematic calibration of a SCARA robot. The discrete motion of each kinematic pair in the robot is completely measured by a coordinate measuring machine. Based on the global kinematic properties of the measured motion, the fixed and moving axes, or guidelines, of the kinematic pairs are identified, which are invariants unrelated to the positions of the measured reference points. The kinematic model of the robot is set up using the identified axes and guidelines. The results validate the approach developed has good efficiency and accuracy.

Introduction

Repeatability and accuracy are important performance indexes of industrial robots. Generally, the geometric errors, including link errors and volumetric errors, take lead responsibilities for the total positioning errors; these cause the robots have satisfactory repeatability but poor accuracy.[1,2] An effective approach to improve accuracy is kinematic calibration,[3–9] which usually contains four steps: modeling, measurement, identification, and implementation.

The modeling step establishes the relationships between the error sources and the actual motion of a robot. A well-known kinematic model is Denavit-Hartenberg (DH) model.[10] However, a standard DH model turned out to be discontinuous in cases of two consecutive parallel kinematic pairs. Some modified models have been proposed to overcome the discontinuity using extra parameters, such as modified DH,[2,11] S,[12] Zero Reference,[13] complete and parametrically continuous,[14,15] and product of exponentials,[16–19] etc. As the additional parameters cause redundancy, sometimes these models may raise the

problem of parameter non-identifiability.[20] In some cases, the simplified DH model[21] has been used to avoid the discontinuity and redundancy. In these models, the geometric errors are equivalent to the link errors, which contain deviations of lengths and orientations of the calibrated links relative to the nominal values. Due to the imperfect geometry of the mating surfaces, the elements of the kinematic pairs, such as rotary axis of revolute pair, move with kinematic pair errors. For an industrial robot, the link errors and the kinematic pair errors have different kinematic properties; both of them influence

[1]School of Mechanical Engineering, Dalian University of Technology, Liaoning, China
[2]Department of Mechanical and Manufacturing Engineering, Aalborg University, Aalborg, Denmark

Corresponding author:
Zhi Wang, School of Mechanical Engineering, Dalian University of Technology, No. 2 Linggong Road, Ganjingzi District, Dalian City, Liaoning Province, P.R.C Dalian, Liaoning 116024, China.
Email: wangzhi@mail.dlut.edu.cn

the accuracy of robots and should be considered for modeling.

The measurement step collects the actual motion of the end link. Many measurement systems are available for this purpose, which can be classified into complete motion measurements and partial motion measurements. The former should measure all the six kinematic parameters of the end link at each discrete measuring position, including three translations and three rotations;[1,22–25] the latter measure partial kinematic parameters of the end link.[26–30] When the robot has redundancy to perform self-motion, the motion of the end link also can be measured using physical constraints, which are claimed to be autonomous and do not require external device.[31–34] According to the measuring principles of the proposed systems, the data measured are trajectories traced by specified points, lines, or planes of the end link. For a three-dimensional motion, the specified trajectories are local properties, which means the identified link errors and kinematic pair errors may be different if the reference points, lines, or planes are different. The global kinematic properties of the measured motion should be discussed and used for kinematic calibration to avoid these differences.

The identification step obtains parameters of the corresponding kinematic models by best fitting the measured motion. Various optimization algorithms have been used, such as least square fitting, Levenberg–Marquardt algorithm and maximum likelihood estimation, etc.[35–40] However, due to large number of optimal variables, which correspond to undetermined parameters of the kinematic models, these algorithms may be low convergence, or convergent to local optimal solutions. On the other hand, because the optimal variables are non-homogeneity for the total errors of the robots, the optimal variables should be assigned different weights. These disadvantages reduce the efficiency and accuracy of identification, especially for the kinematic model with numerous parameters.

In this work, both link errors and kinematic pair errors are considered for kinematic calibration of industrial robots. The kinematic pair errors are defined as the error motions of the moving element relative to the fixed one, e.g., the revolute pair errors are defined as the error motions of the moving axis relative to the fixed axis.[41] To avoid the differences caused by different reference points or lines, a new approach, based on the invariants of the measured motion, is presented to determine the fixed and moving axes of revolute pairs, or the guidelines of prismatic pairs. The errors of each link and kinematic pair are identified individually to overcome low convergence and non-homogeneity in identification. A SCARA robot is taken as an example to illustrate the proposed approach, whose kinematic model is set up using the identified moving and fixed elements. With the proposed model, both link errors and kinematic pair errors of the SCARA robot are identified and the link errors are compensated.

Errors of kinematic pairs

The errors of kinematic pairs are presented due to the imperfect geometry of the mating surfaces in kinematic pairs. In a revolute pair, the center lines of the shaft and the housing are not coincident, and neither of them is exactly the rotary axis. In a prismatic pair, the center lines of the two relative translational links are not exactly the line of translation. In the following, the errors of the revolute pair and prismatic pair are discussed independently, based on the global kinematic properties of the discrete error motion.

Trajectories of points and lines

In error modeling of 3D mechanism, the motion of the moving link $i+1$ of a kinematic pair K_{i+1} relative to the other link i will have six degree of freedoms (DOFs). This motion can be described with three translations $(x_{i+1}, y_{i+1}, z_{i+1})$ and three rotations $(\alpha_{i+1}, \beta_{i+1}, \gamma_{i+1})$ of frame $\{O_{i+1}; i_{i+1}, j_{i+1}, k_{i+1}\}$ attached to link $i+1$ relative to frame $\{O_i; i_i, j_i, k_i\}$ attached to link i, as shown in Figure 1. To identify the kinematic pair errors of K_{i+1}, all the six kinematic parameters should be measured by the measurement step. In the following pages, frame $\{O_i; i_i, j_i, k_i\}$ is abbreviated to frame i for short.

The undesired motion is caused by the link errors and the kinematic pair errors. Take a revolute pair for example; there have a moving axis of rotation S_{i+1}^b and a fixed axis S_i^a in the revolute pair, the former belongs to link $i+1$ and the latter belongs to link i. In ideal case, these two axes are coincident with the geometric axis of the shaft or the housing, but in real systems, they have offset from each other and both of them are not coincident with the geometric axis due to manufacturing errors and deformations. The deviations of position and orientation of fixed axis S_i^a relative to the designed axis in frame i describe the errors of link i, while the motion of moving axis S_{i+1}^b relative to fixed
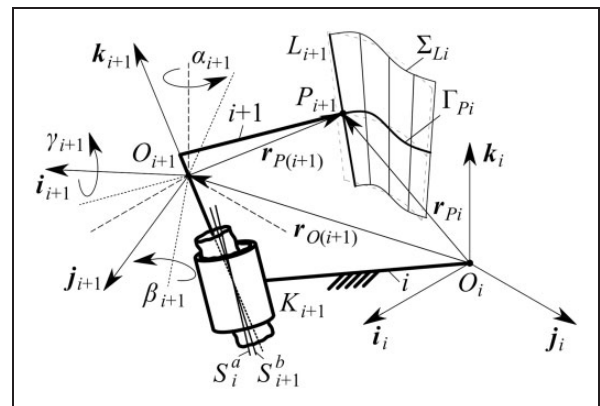

Figure 1. The actual motion of a revolute pair.

axis S_i^a describes the errors of revolute pair K_{i+1}. The key issue of error identification is how to locate the moving and fixed elements of the kinematic pairs, such as the axes of rotation of revolute pair and the guidelines of translation of prismatic pair.

The trajectories traced by points and lines of the moving link reveal the kinematic and geometric properties of the motion, which can be used to locate the axes or guidelines of the kinematic pairs. As moving link $i+1$ moves, a point P_{i+1} of the link traces a spatial curve Γ_{Pi} in frame i, whose vector equation can be written as[42]:

$$\Gamma_{Pi} : r_{Pi} = r_{O(i+1)} + [^{i+1}R_i]r_{P(i+1)} \qquad (1)$$

where r_{Pi} is the coordinate vector of point P_{i+1} on curve Γ_{Pi} in frame i; $r_{O(i+1)} = [x_{i+1}, y_{i+1}, z_{i+1}]^T$ is the displacement vector of the origin point O_{i+1} in frame i; $r_{P(i+1)}$ is the coordinate vector of point P_{i+1} in frame $i+1$; the subscripts i and $i+1$ denote the number the links. $[^{i+1}R_i]$ is the rotational matrix from frame $i+1$ to frame i, whose value is:

$$[^{i+1}R_i] = \begin{bmatrix} c\alpha_{i+1} & -s\alpha_{i+1} & 0 \\ s\alpha_{i+1} & c\alpha_{i+1} & 0 \\ 0 & 0 & 1 \end{bmatrix} \begin{bmatrix} c\beta_{i+1} & 0 & s\beta_{i+1} \\ 0 & 1 & 0 \\ -s\beta_{i+1} & 0 & c\beta_{i+1} \end{bmatrix}$$
$$\times \begin{bmatrix} 1 & 0 & 0 \\ 0 & c\gamma_{i+1} & -s\gamma_{i+1} \\ 0 & s\gamma_{i+1} & c\gamma_{i+1} \end{bmatrix} \qquad (2)$$

where α_{i+1}, β_{i+1}, and γ_{i+1} are *k-j-i* Euler angles, as shown in Figure 1. Letters c and s denote cosine and sine for short.

A line L_{i+1} of the moving link $i+1$, passing the point P_{i+1}, traces a ruled surface Σ_{Li} in frame i, and the vector equation of the trajectory Σ_{Li} can be written as:

$$\Sigma_{Li} : r_{Li} = \rho_i + \lambda_\rho l_i; \quad \rho_i = r_{Pi} + b_L l_i, \quad l_i = [^{i+1}R_i]l_{i+1} \qquad (3)$$

In above equation, r_{Li} is the coordinate vector of Σ_{Li} in frame i; ρ_i is the striction point vector; and l_i is the unit direction vector of the rectilinear generator L_{i+1} on Σ_{Li};[42] λ_ρ is the line variable and l_{i+1} is the unit direction vector of line L_{i+1} in frame $i+1$; r_{Pi} and $[^i+1R_i]$ are the same as equation (1), and r_{Pi} is the directrix vector; b_L is distance from the striction point to the directrix. As a matter of fact, the motion of the link is measured in a series of discrete positions; hence, the line-trajectory can be rewritten in a standard discrete form:

$$\Sigma_{Li}^{(t)} : r_{Li}^{(t)} = \rho_i^{(t)} + \lambda_\rho l_i^{(t)}; \quad t = 1, \ldots, n \qquad (4)$$

The parameters in equation (4) are the same as those in equation (3) with discrete forms. The point

sets $\{\rho_i^{(t)}\}$ and $\{l_i^{(t)}\}$ are discrete striction curve and discrete spherical image curve of $\Sigma_{Li}^{(t)}$.

As known from the kinematic geometry,[43] both striction curve and spherical image curve are invariants of a line-trajectory, and completely describe the geometric properties of a line-trajectory. We can use the spherical image curve error and striction curve error to describe the orientation error and position error of a line-trajectory. Furthermore, the spherical image curves and striction curves of the line-trajectories traced by all lines of the moving link reveal the global geometric properties of the motion of a kinematic pair.

The errors of a revolute pair

An ideal revolute pair constrains five DOFs except nominal rotation. According to the Wang et al.,[42] Wang and Wang,[43] and Wang et al.,[44] the trajectory traced by a line of the moving link is a hyperboloid of one sheet, a circular conical surface or a cylindrical surface; this means the spherical image curve of the line-trajectory is a spherical image circle or point and the striction curve is a circle or point. The moving and fixed axes of the revolute pair are coincident with the geometric axis of the ideal line-trajectory.

In an actual revolute pair, the moving link rotates with kinematic pair errors; the trajectory traced by a line of the moving link is approximated to the ideal one, as the kinematic pair errors are much smaller than the nominal rotation in magnitude. Hence, an ideal hyperboloid of one sheet is taken to fit the actual discrete line-trajectory, in order to identify its orientation and position errors caused by the kinematic pair errors. The surface fitting can be realized by two curve fittings in sequence, the spherical image circle fitting of the actual spherical image curve $\{l_i^{(t)}\}$ and the circle fitting of the actual striction curve $\{\rho_i^{(t)}\}$. For instance, the line-trajectory described by equation (4) is divided into a discrete spherical image curve and a discrete striction curve; these two discrete curves can be fitted in sequence as follows.

The discrete spherical image curve $\{l_i^{(t)}\}$ of the line-trajectory, traced by an arbitrary line of the moving link $i+1$, is fitted by a self-adaption spherical image circle with the minimal fitting error. In order to avoid the influences caused by the total number of the discrete positions used, the approach of saddle point programming is used. The mathematic model is:

$$\begin{cases} \min_{a} \max_{1 \leqslant t \leqslant n} g_a^{(t)}(a) = \left| \arccos(S_i^a \cdot l_i^{(t)}) - \delta_{si} \right| \\ S_i^a = [\sin\eta_{si}\cos\xi_{si}, \sin\eta_{si}\sin\xi_{si}, \cos\eta_{si}]^T \\ a = (\eta_{si}, \xi_{si}, \delta_{si})^T \\ s.t. \ \eta_{si} \in [0, \pi), \xi_{si} \in [0, 2\pi), \delta_{si} \in [0, \pi/2] \end{cases} \qquad (5)$$

where $g_a^{(t)}(a)$ is the optimization function. The optimization variables a contain direction angles (η_{si}, ξ_{si})
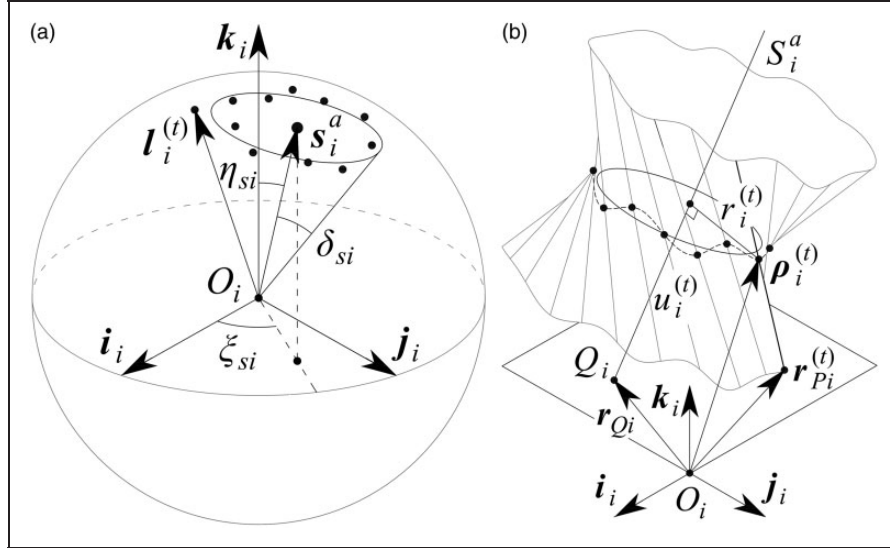
Figure 2. The spherical image circle fitting and striction circle fitting of a line-trajectory. (a) Spherical image circle fitting and (b) striction circle fitting.

of the unit direction vector S_i^a and half-cone angle δ_{si} of the cone formed by the center of the sphere and the fitting spherical image circle, as shown in Figure 2(a). S_i^a is the unit direction vector of the geometric axis of the fitting circle. The fitting error, denoted as Δ_D, is defined as the spherical image curve error of the line-trajectory. n is the number of the discrete lines.

The spherical image circle fitting locates the orientation of geometric axis S_i^a and identifies the orientation error of the revolute pair. Then, in order to locate the position of the geometric axis and identify the position error, the discrete striction curve $\{\rho_i^{(t)}\}$ is fitted using a self-adaption striction circle with the minimal fitting error. The mathematic model of striction circle fitting with the saddle point programming is written as:

$$
\begin{cases}
\min_{b} \max_{1 \leqslant t \leqslant n} g_b^{(t)}(\boldsymbol{b}) = \sqrt{\left(r_i^{(t)} - r_{i0}\right)^2 - \left(u_i^{(t)} - u_{i0}\right)^2} \\
r_i^{(t)} = (\rho_i^{(t)} - \boldsymbol{r}_{Qi}) \dfrac{\boldsymbol{l}_i^{(t)} \times S_i^a}{|\boldsymbol{l}_i^{(t)} \times S_i^a|}; \; u_i^{(t)} = (\rho_i^{(t)} - \boldsymbol{r}_{Qi}) S_i^a \\
\boldsymbol{b} = \left(x_{Qi}, y_{Qi}, r_{i0}, u_{i0}\right)^T \\
s.t. \; r_i \in (0, +\infty); \; x_{Qi}, y_{Qi}, u_{i0} \in (-\infty, +\infty)
\end{cases}
\tag{6}
$$

where $g_b^{(t)}(\boldsymbol{b})$ is the optimization function. The optimization variables (x_{Qi}, y_{Qi}) are coordinates of the position vector $\boldsymbol{r}_{Qi} = [x_{Qi}, y_{Qi}, 0]^T$ of the reference point Q_i on geometric axis S_i^a in frame i; r_{i0} is the radius of the fitting circle and u_{i0} is the distance from point Q_i to the center of the fitting circle, as shown in Figure 2(b). $r_i^{(t)}$ is the radial distance between striction point $\rho_i^{(t)}$ and axis S_i^a; $u_i^{(t)}$ is the axial distance between striction point $\rho_i^{(t)}$ and the projective point of Q_i along axis S_i^a. S_i^a is the optimization result of equation (5). The fitting error, denoted as Δ_L, is regarded as the striction curve error of the line-trajectory. The striction point $\rho_i^{(t)}$ of the line-trajectory

can be calculated by:

$$
\rho_i^{(t)} = \boldsymbol{r}_{Pi}^{(t)} + b_L^{(t)} \boldsymbol{l}_i^{(t)}
\tag{7}
$$

The parameters in equation (7) are the same as those in equation (3) with discrete forms; and the value of $b_L^{(t)}$ is:

$$
b_L^{(t)} = \frac{(\boldsymbol{r}_{Qi} - \boldsymbol{r}_{Pi}^{(t)}) \cdot [\boldsymbol{l}_i^{(t)} - (\boldsymbol{l}_i^{(t)} \cdot S_i^a) S_i^a]}{1 - \left(\boldsymbol{l}_i^{(t)} \cdot S_i^a\right)^2}
\tag{8}
$$

Generally, a specific line of the moving link $i+1$, denoted as S_{i+1}^b, whose fitting errors Δ_D and Δ_L are the smallest of all lines L_{i+1} of link $i+1$, can be obtained and regarded as the moving axis of the revolute pair. Meanwhile, the fitting axis S_i^a of the line-trajectory, traced by axis S_{i+1}^b, is treated as the fixed axis of the revolute pair. The kinematic pair errors of the revolute pair can be defined as the error motion of the moving axis relative to the fixed axis, while the link errors are defined as the deviations between the fixed axis and the designated axis. In comparing with the errors proposed in the existing models, the minimal spherical image curve error and the minimal striction curve error are independent to the positions and orientations of the reference coordinate frames, or the reference points and lines measured, which bring in great advantages for the motion measurement and error identification. On the other hand, these two errors have the minimal values, which are beneficial to improve the accuracy of error compensation.

The errors of a prismatic pair

An ideal prismatic pair constrains five DOFs except nominal translation. The trajectory traced by a line of the moving link is a plane; the striction curve of the
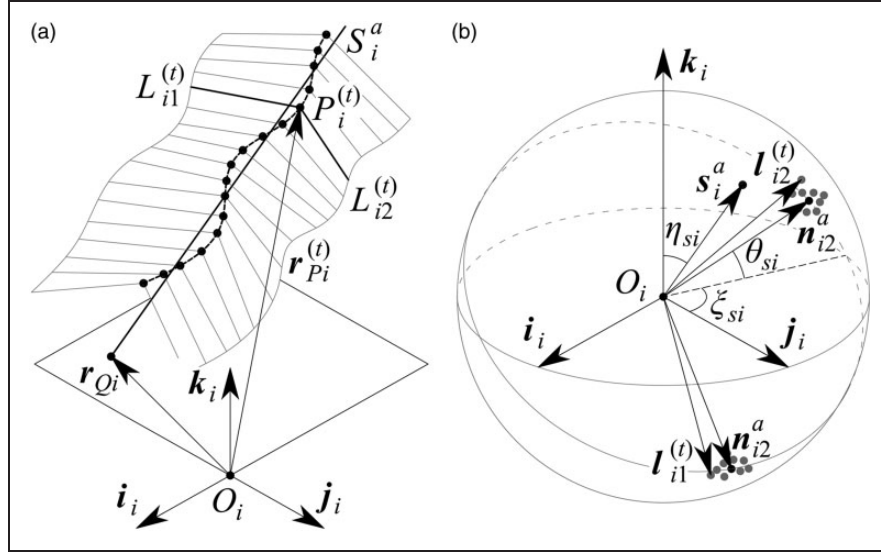
Figure 3. The line fitting and spherical points fitting of point- and line-trajectories. (a) Line fitting and (b) spherical points fitting.

line-trajectory degenerates to a straight line traced by a point of the moving link, and this striction curve is parallel to the moving and fixed guidelines of the prismatic pair.[45]

In an actual prismatic pair, the moving link moves with prismatic pair errors; the trajectory traced by a point is approximate to the straight line, as the prismatic pair errors are much smaller than the nominal translation in magnitude. A straight line is taken to fit the actual point-trajectory, in order to identify its errors and locate its approximate guideline. The approach of saddle point programming is employed to make the fitting error be smallest, and the mathematic model can be written as:

$$\begin{cases} \min_{\mathbf{c}} \max_{1 \leqslant t \leqslant n} g_c^{(t)}(\mathbf{c}) = \left| \mathbf{r}_{Pi}^{(t)} - \mathbf{r}_{Qi} - (\mathbf{r}_{Pi}^{(t)} - \mathbf{r}_{Qi}) \cdot S_i^a \cdot S_i^a \right| \\ S_i^a = [\sin \eta_{si} \cos \xi_{si}, \ \sin \eta_{si} \sin \xi_{si}, \ \cos \eta_{si}]^T \\ \mathbf{c} = \left(x_{Qi}, y_{Qi}, \eta_{si}, \xi_{si} \right)^T \\ s.t. \ x_{Qi}, y_{Qi} \in (-\infty, +\infty); \ \eta_{si} \in [0, \pi); \ \xi_{si} \in [0, 2\pi) \end{cases}$$
(9)

where $g_c^{(t)}(\mathbf{c})$ is the optimization function. The optimization variables (x_{Qi}, y_{Qi}) are coordinates of the position vector $\mathbf{r}_{Qi} = [x_{Qi}, y_{Qi}, 0]^T$ of reference point Q_i on guideline S_i^a in frame i; η_{si} and ξ_{si} are the direction angles of line S_i^a; $\mathbf{r}_{Pi}^{(t)}$ is the coordinate vector of $P_i^{(t)}$ in frame i, whose value can be calculated by equation (1) with a discrete form, as shown in Figure 3(a). The fitting error, denoted as Δ_L, is defined as the position error of the trajectory, or the directrix error, as the point-trajectory is a directrix of a line-trajectory. n is the total number of the discrete positions.

In general, a specific point of the moving link $i+1$, denote as P_{i+1}^b, can be obtained by minimizing the fitting error Δ_L of all points P_{i+1} of link $i+1$, and regarded as the reference point of the moving guideline. Meanwhile, the fitting line S_i^a of the

point-trajectory, traced by point P_{i+1}^b, is regarded as the fixed guideline of the prismatic pair.

The line fitting of point-trajectory locates the fixed guideline and identifies the position error of the prismatic pair. Then, in order to locate the orientation of the moving guideline and identify the orientation error of the prismatic pair, two unit direction vectors $\mathbf{n}_{i1}^a$ and $\mathbf{n}_{i2}^a$, perpendicular to S_i^a, are taken to fit the discrete spherical image curves of two line sets $\{L_{i1}^{(t)}\}$ and $\{L_{i2}^{(t)}\}$, traced by two perpendicular lines of the moving link. Here, two unit direction vectors are employed because two nonparallel vectors are needed to locate the posture of a moving link at least. The model is:

$$\begin{cases} \min_{\mathbf{d}} \max_{1 \leqslant t \leqslant n} g_d^{(t)}(\mathbf{d}) = \left| \arccos(\mathbf{n}_{i1}^a \cdot \mathbf{l}_{i1}^{(t)}) \right| + \left| \arccos(\mathbf{n}_{i2}^a \cdot \mathbf{l}_{i2}^{(t)}) \right| \\ \mathbf{n}_{i1}^a = (c\xi_{si} c\eta_{si} c\theta_{si} - s\xi_{si} s\theta_{si}, s\xi_{si} c\eta_{si} c\theta_{si} + c\xi_{si} s\theta_{si}, -s\eta_{si} c\theta_{si})^T \\ \mathbf{n}_{i2}^a = (-c\xi_{si} c\eta_{si} s\theta_{si} - s\xi_{si} c\theta_{si}, -s\xi_{si} c\eta_{si} s\theta_{si} + c\xi_{si} c\theta_{si}, s\eta_{si} s\theta_{si})^T \\ \mathbf{d} = (\eta_{si}, \xi_{si}, \theta_{si})^T \\ s.t. \ \eta_{si} \in [0, \pi), \xi_{si} \in [0, 2\pi), \theta_{si} \in [0, 2\pi) \end{cases}$$
(10)

where $g_d^{(t)}(\mathbf{d})$ is the optimization function. The optimization variables $(\eta_{si}, \xi_{si}, \theta_{si})$ are the Euler angles shown in Figure 3(b). The minimal fitting error, denoted as Δ_D, is defined as the spherical image curve error.

For all lines of moving link $i+1$, two perpendicular lines with the unit direction vectors denoted by $\mathbf{l}_{(i+1)1}^b$ and $\mathbf{l}_{(i+1)2}^b$, can be obtained by the minimizing fitting error Δ_D. These two vectors can be regarded as the unit normal vectors of the moving guide planes of the prismatic pair, and the vectors $\mathbf{n}_{i1}^a$ and $\mathbf{n}_{i2}^a$ are regarded as the unit normal vectors of the fixed guide planes of the prismatic pair. A line S_{i+1}^b of link $i+1$, across point P_{i+1}^b with unit direction vector $S_{i+1}^b = \mathbf{l}_{(i+1)1}^b \times \mathbf{l}_{(i+1)2}^b$, is regarded as the moving guideline of the prismatic pair. Hence, the kinematic pair
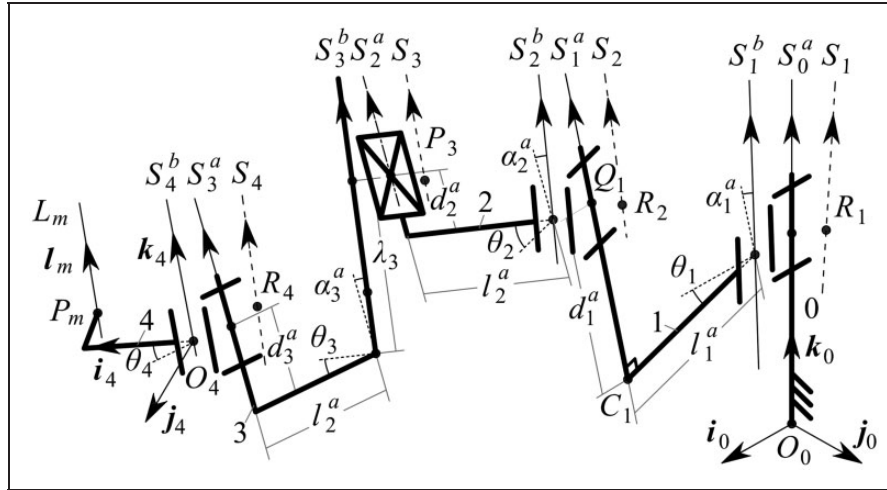
Figure 4. The kinematic model of the SCARA robot.

errors of the prismatic pair can be defined as the error motions of the moving guideline and planes relative to the fixed guideline and planes, and the link errors are defined as the deviations of the fixed guideline and planes to the designated one. Similar to the revolute pair errors, the two identified errors of the prismatic pair are independent to the positions and orientations of the reference coordinate frames, or the reference points and lines measured. Both of them have the minimal values.

Kinematic model of a SCARA robot

We apply the developed method to a SCARA robot, which contains three revolute pairs R_1, R_2, R_4, and one prismatic pair P_3. As discussed, a revolute pair has an approximate fixed axis S_i^a and an approximate moving axis S_{i+1}^b, but not the designated axis S_i. Similarly, there have an approximate fixed guideline S_i^a and an approximate moving guideline S_{i+1}^b in a prismatic pair. The kinematic model of the robot can be established based on the axes and guidelines, as shown in Figure 4.

The parameters of the kinematic model follow the D-H conventions. For each link i, it has three structure parameters, which will be calculated if the axes or guidelines of the kinematic pairs are determined. The length l_i^a is the normal distance between axis S_i^b of the former kinematic pair and axis S_i^a of the latter one, while the deflection angle α_i^a is the angle from S_i^b to S_i^a; d_i^a is the distance from pedal C_i to reference point Q_i. Thus, the transformation matrix $[T_i^a]$ of link i can be written as:

$$[T_i^a] = \begin{bmatrix} 1 & 0 & 0 & l_i^a \\ 0 & c\alpha_i^a & -s\alpha_i^a & d_i^a s\alpha_i^a \\ 0 & s\alpha_i^a & c\alpha_i^a & d_i^a c\alpha_i^a \\ 0 & 0 & 0 & 1 \end{bmatrix} \quad (11)$$

The parameters in $[T_i^a]$ are shown in Figure 4.

The transformation matrix $[^{i+1}T_i^{(t)}]$ from frame $i+1$ to frame i can be written as:

$$[^{i+1}T_i^{(t)}] = \begin{bmatrix} [^{i+1}R_i^{(t)}] & r_{O(i+1)}^{(t)} \\ 0 & 1 \end{bmatrix} \quad (12)$$

$[^{i+1}R_i^{(t)}]$ and $r_{O(i+1)}^{(t)}$ are the same as equation (1) with discrete forms, which are determined by the six kinematic parameters of moving link $i+1$ and measured in the measurement step. As $[^{i+1}T_i^{(t)}]$ is composed by the transformation matrixes of link $i+1$ and kinematic pair $i+1$, it can be rewritten as:

$$[^{i+1}T_i^{(t)}] = [T_i^a][^{i+1}T_i^{b(t)}] \quad (13)$$

where $[^{i+1}T_i^{b(t)}]$ is transformation matrix of kinematic pair $i+1$ at discrete position (t), which can be calculated by equations (11)–(13).

According to the kinematic model, the trajectory of a function line L_{F4} of the end link 4 in frame $\{O_0; i_0, j_0, k_0\}$ is:

$$\Sigma_{LF} : r_{LF}^{(t)} = r_{PF}^{(t)} + \lambda l_F^{(t)}; \quad \begin{bmatrix} r_{PF}^{(t)} \\ 1 \end{bmatrix} = [^4T_0^{(t)}]\begin{bmatrix} r_{PF4} \\ 1 \end{bmatrix},$$

$$\begin{bmatrix} l_F^{(t)} \\ 0 \end{bmatrix} = [^4T_0^{(t)}]\begin{bmatrix} l_{F4} \\ 0 \end{bmatrix} \quad (14)$$

where r_{PF4} and l_{F4} are the coordinate vector of point P_{F4} and the unit direction vector of line L_{F4} in frame $\{O_4; i_4, j_4, k_4\}$. The transformation matrix $[^4T_0^{(t)}]$ can be calculated by:

$$[^4T_0] = \prod_{i=0}^{3} [^{i+1}T_i^{(t)}] \quad (15)$$

Generally, the kinematic pair errors are difficult to be compensated, as they are changing with the

configurations of the robots. For kinematic calibration, when the identified kinematic pair errors are much smaller than the link errors, the matrix $[^{i+1}\boldsymbol{T}_i^{(t)}]$ can be simplified to:

$$^{i-1}\boldsymbol{T}_i^{(t)} = \begin{bmatrix} c\theta_i^{(t)} & -c\alpha_i^a s\theta_i^{(t)} & s\alpha_i^a s\theta_i^{(t)} & l_i^a c\theta_i^{(t)} + d_i^a s\alpha_i^a s\theta_i^{(t)} \\ s\theta_i^{(t)} & c\alpha_i^a c\theta_i^{(t)} & -s\alpha_i^a c\theta_i^{(t)} & l_i^a s\theta_i^{(t)} - d_i^a s\alpha_i^a c\theta_i^{(t)} \\ 0 & s\alpha_i^{(j)} & c\alpha_i^a & \lambda_i^{(t)} + d_i^a c\alpha_i^a \\ 0 & 0 & 0 & 1 \end{bmatrix}$$
(16)

where $\theta_i^{(t)}$ and $\lambda_i^{(t)}$ are the driving parameters of the revolute pairs and prismatic pairs.

machine (CMM, ZEISS-MMZ-G30-40-20); then, the coordinate vector of the center point $\boldsymbol{r}_{Bu}$ of B_u can be calculated as:

$$\boldsymbol{r}_{Bu}^{(t)} = [x_{Bu}^{(t)}, y_{Bu}^{(t)}, z_{Bu}^{(t)}]^T = [\boldsymbol{A}_u^{(t)}]^{-1}[\boldsymbol{B}_u^{(t)}]$$
(17)

where the subscript u denotes the number of the ball. Matrixes $[\boldsymbol{A}_u^{(t)}]$ and $[\boldsymbol{B}_u^{(t)}]$ are written as:

$$[\boldsymbol{A}_u^{(t)}] = \begin{bmatrix} x_{u2}^{(t)} - x_{u1}^{(t)} & y_{u2}^{(t)} - y_{u1}^{(t)} & z_{u2}^{(t)} - z_{u1}^{(t)} \\ x_{u3}^{(t)} - x_{u1}^{(t)} & y_{u3}^{(t)} - y_{u1}^{(t)} & z_{u3}^{(t)} - z_{u1}^{(t)} \\ x_{u4}^{(t)} - x_{u1}^{(t)} & y_{u4}^{(t)} - y_{u1}^{(t)} & z_{u4}^{(t)} - z_{u1}^{(t)} \end{bmatrix}$$
(18)

$$[\boldsymbol{B}_u^{(t)}] = \begin{bmatrix} (x_{u2}^{(t)} - x_{u1}^{(t)})(x_{u2}^{(t)} + x_{u1}^{(t)}) + (y_{u2}^{(t)} - y_{u1}^{(t)})(y_{u2}^{(t)} + y_{u1}^{(t)}) + (z_{u2}^{(t)} - z_{u1}^{(t)})(z_{u2}^{(t)} + z_{u1}^{(t)}) \\ (x_{u3}^{(t)} - x_{u1}^{(t)})(x_{u3}^{(t)} + x_{u1}^{(t)}) + (y_{u3}^{(t)} - y_{u1}^{(t)})(y_{u3}^{(t)} + y_{u1}^{(t)}) + (z_{u3}^{(t)} - z_{u1}^{(t)})(z_{u3}^{(t)} + z_{u1}^{(t)}) \\ (x_{u4}^{(t)} - x_{u1}^{(t)})(x_{u4}^{(t)} + x_{u1}^{(t)}) + (y_{u4}^{(t)} - y_{u1}^{(t)})(y_{u4}^{(t)} + y_{u1}^{(t)}) + (z_{u4}^{(t)} - z_{u1}^{(t)})(z_{u4}^{(t)} + z_{u1}^{(t)}) \end{bmatrix}$$
(19)

Kinematic calibration of a SCARA robot

Measurements of discrete motions

A SCARA robot used for twisting screws are taken to illustrate the proposed approach, as shown in Figure 5(a). The nominal lengths of arms l_1 and l_2 are designed as 250 mm and 400 mm, and the travels of the kinematic pairs R_1, R_2, P_3, and R_4 are 120°, 260°, 180 mm, and 160°, respectively.

An artifact with five balls (sphericity less than 0.5 μm) is fixed to the end link of the robot, and the coordinates of the center points of the balls are measured at each discrete position (t) to obtain the discrete motions of the end link 4. For each ball B_u, the coordinates of four non-coplanar points B_{uv} on the surface are measured by a coordinate measuring

Parameters $(x_{uv}^{(t)}, y_{uv}^{(t)}, z_{uv}^{(t)})$ are the coordinates of points B_{uv} ($v = 1, 2, 3, 4$) measured by the CMM.

As know from the kinematic geometry,[43] the discrete motion of a link can be determined by the coordinates of three non-collinear points of the link. Thus, the coordinates of the center points of three balls B_1, B_3, and B_5 are used to determine the position and orientation of the end link, which can be described by a coordinate frame $\{O_B; \boldsymbol{i}_B, \boldsymbol{j}_B, \boldsymbol{k}_B\}$ attached to the artifact on link 4 as:

$$\boldsymbol{r}_{OB}^{(t)} = \boldsymbol{r}_{B3}^{(t)}; \boldsymbol{i}_B^{(t)} = \frac{\boldsymbol{r}_{B3}^{(t)} - \boldsymbol{r}_{B1}^{(t)}}{|\boldsymbol{r}_{B3}^{(t)} - \boldsymbol{r}_{B1}^{(t)}|};$$
$$\boldsymbol{k}_B^{(t)} = \frac{(\boldsymbol{r}_{B3}^{(t)} - \boldsymbol{r}_{B1}^{(t)}) \times (\boldsymbol{r}_{B5}^{(t)} - \boldsymbol{r}_{B1}^{(t)})}{\left|(\boldsymbol{r}_{B3}^{(t)} - \boldsymbol{r}_{B1}^{(t)}) \times (\boldsymbol{r}_{B5}^{(t)} - \boldsymbol{r}_{B1}^{(t)})\right|}; \quad \boldsymbol{j}_B^{(t)} = \boldsymbol{k}_B^{(t)} \times \boldsymbol{i}_B^{(t)}$$
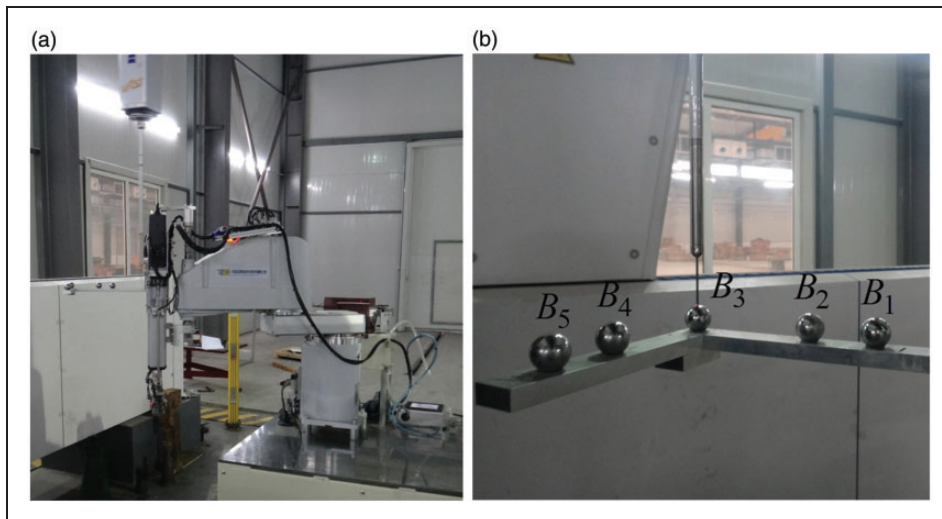(20)

Figure 5. Measurements of discrete motions. (a) The SCARA robot and (b) artifact with five balls.

The discrete motion represented by the six kinematic parameters of link 4 can be calculated as:

$$\begin{cases} [x_B^{(t)}, y_B^{(t)}, z_B^{(t)}]^T = \boldsymbol{r}_{B3}^{(t)} \\ \begin{cases} \alpha_B^{(t)} = \text{atan2}(i_{B2}^{(t)}, i_{B1}^{(t)}); \\ \beta_B^{(t)} = \text{atan2}\left(-i_{B3}^{(t)}, \sqrt{(i_{B1}^{(t)})^2 + (i_{B2}^{(t)})^2}\right); \\ \gamma_B^{(t)} = \text{atan2}(j_{B3}^{(t)}, k_{B3}^{(t)}) \end{cases} \end{cases} \quad (21)$$

where atan2 denotes the double parameters arctangent function. Variables $i_{Bk}^{(t)}$, $j_{Bk}^{(t)}$, and $k_{Bk}^{(t)}$ are the kth elements of vectors $\boldsymbol{i}_B^{(t)}$, $\boldsymbol{j}_B^{(t)}$, and $\boldsymbol{k}_B^{(t)}$, respectively.

The discrete motions of end link 4 generated by kinematic pairs R_1, R_2, P_3, and R_4 are measured, respectively, and the displacements of the frame $\{O_B; \boldsymbol{i}_B, \boldsymbol{j}_B, \boldsymbol{k}_B\}$ in the measuring coordinates frame are shown in Appendix 1 at the end of this paper. The kinematic pairs are controlled independently in measurements, which means when measuring one kinematic pair, the other kinematic pairs are locked at the initial positions. For each kinematic pair, we choose 11 equi-spaced discrete positions to determine the axes or guidelines. The process of the kinematic calibration is shown in Figure 6.

Error identification of the robot

For an arbitrary line of link 4 with position vector $\boldsymbol{r}_{P4}$ and unit direction vector $\boldsymbol{l}_4$, its trajectory in frame

$\{O_0; \boldsymbol{i}_0, \boldsymbol{j}_0, \boldsymbol{k}_0\}$ will be calculated by equations (1) to (4), when the six kinematic parameters of link 4 are measured. Then, the trajectories traced by all lines of link 4 are obtained and their errors are calculated by equations (5) to (10). The fixed axes or guidelines of the kinematic pairs in frame $\{O_0; \boldsymbol{i}_0, \boldsymbol{j}_0, \boldsymbol{k}_0\}$ are located and the corresponding kinematic pair errors are identified by searching the minimal errors. The results are shown in Table 1.

The trajectory of the function line L_{F4} ($\boldsymbol{r}_{PF4} = [0,0,0]^T$, $\boldsymbol{l}_{F4} = [0,0,1]^T$) of the end link is used for error analysis, as the position and orientation of the axis of the screw are concerned for twisting a screw. For instance, 10 poses of a circular trajectory are chosen, and the equation of the nominal poses is:

$$\boldsymbol{r}_F = \left[350\cos\frac{n\pi}{18} + 100, 350\frac{n\pi}{18}, 485\right]^T + \lambda[0, 0, 1]^T;$$
$$n = \pm1, \pm2, \ldots, \pm5 \quad (22)$$

Due to errors, the poses of the function line are different from the nominal one. The deviations of positions and orientations are regarded as the total errors of the SCARA robot, which are measured by the CMM. The link errors are calculated by equations (11) to (16) with the identified fixed axes and guideline, and the kinematic pair errors are the additional errors, which correspond to the errors of the line-trajectories in the discrete positions. The positions and orientations errors of the discrete trajectory of
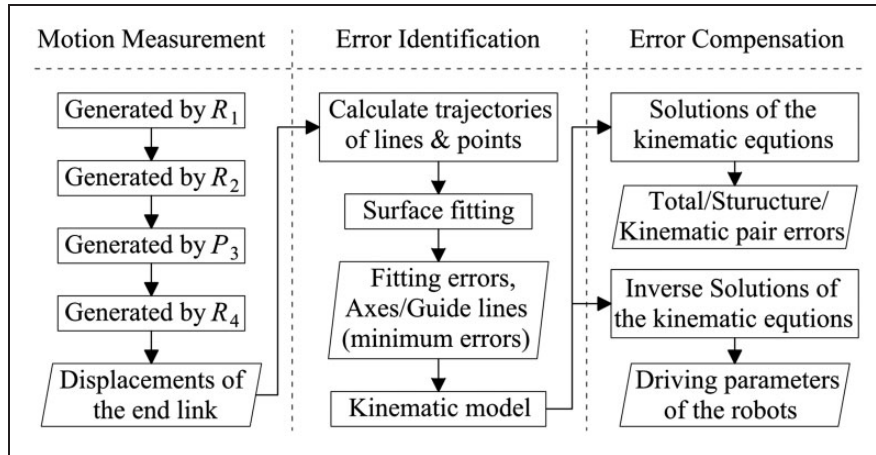
Figure 6. The process of the kinematic calibration.

Table 1. The fixed element and errors of the kinematic pairs.

	x_{Qi}/mm	y_{Qi}/mm	ξ_{si}/rad	η_{si}/rad	Δ_D/rad	Δ_L/μm
R_1	0	0	0	0	3.32×10^{-5}	4.56
R_2	250.458	0	2.5256	9.4253×10^{-4}	1.37×10^{-4}	10.96
P_3	1079.071	53.889	-0.5605	1.4607×10^{-3}	5.98×10^{-5}	12.63
R_4	649.804	1.254	0.8867	1.0347×10^{-3}	3.67×10^{-5}	11.53

the function line are shown in Figure 7(a) and 7(b), respectively.

The results show the total errors of the robot are mainly caused by the link errors, which means the accuracy of the SCARA robot may be improved considerably if the link errors are compensated properly. In comparing with the existing identification approaches, the identifications of the fixed and moving elements are based on the measured motion generated by each kinematic pair. Thus, the identification models are unrelated to the kinematic model of the robot; this improves the efficiency of error identification and there is no need to assign weights for different parameters.

Error compensation of the robot

The link errors are invariable as the loads of the robot change if the stiffness of the links is large enough; hence, these errors can be compensated by inverse solution of the equation (14). Based on the identified parameters, the configurations θ_1, θ_2, and λ_3 of the ideal robot corresponded to the 10 poses of equation (22) and the configurations θ_1^a, θ_2^a, and λ_3^a of the actual robot corresponded to the same poses after compensation are shown in Table 2.

The position and orientation errors of the function line along a discrete line-trajectory before and after compensation are shown in Figure 8(a) and 8(b), respectively.

A line-trajectory is taken to observe the effect of compensation when the revolute pairs and the prismatic pair are moving together. The coordinates (x_F, y_F, z_F) of the function point of the end link in frame $\{O_0; i_0, j_0, k_0\}$ and the corresponding configurations of the actual robot after compensation are shown in

Table 2. The configurations of the robot before and after compensation.

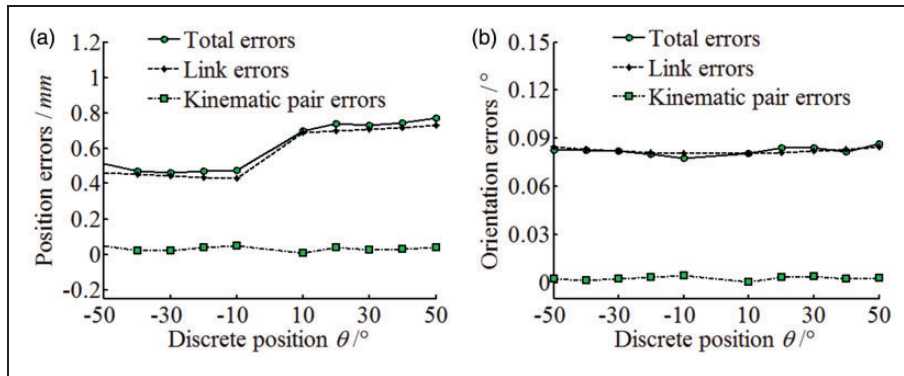| Without compensation			After compensation		
$\theta_1/°$	$\theta_2/°$	λ_3/mm	$\theta_1^a/°$	$\theta_2^a/°$	λ_3^a/mm
28.158	−103.004	−15.000	28.073	−102.897	−15.164
34.311	−100.479	−15.000	34.227	−100.372	−15.149
40.736	−98.447	−15.000	40.653	−98.340	−15.137
47.492	−96.956	−15.000	47.409	−96.850	−15.129
54.626	−96.045	−15.000	54.544	−95.939	−15.123
−54.626	96.045	−15.000	−54.665	96.135	−15.557
−47.492	96.956	−15.000	−47.530	97.046	−15.561
−40.736	98.447	−15.000	−40.774	98.536	−15.569
−34.311	100.479	−15.000	−34.348	100.569	−15.578
−28.158	103.004	−15.000	−28.194	103.093	−15.590

Figure 7. The position errors and orientation errors of the function line. (a) The position errors and (b) the orientation errors.
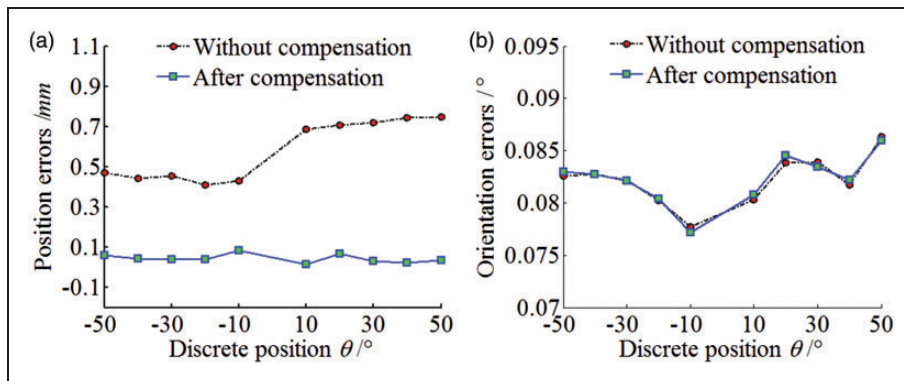

Figure 8. The motion errors before and after compensation. (a) The position errors and (b) the orientation errors.

Table 3. The coordinates of the function point and the configurations of the robot.

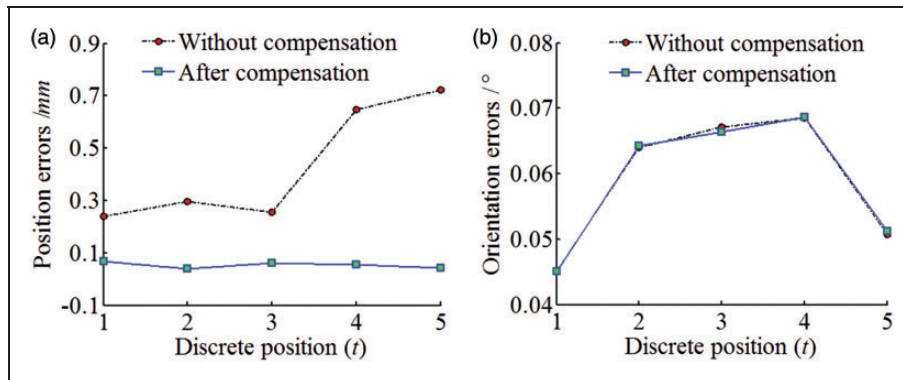| x_F/mm	y_F/mm	z_F/mm	$\theta_1^a/°$	$\theta_2^a/°$	λ_3^a/mm
500,000	−300,000	−15,000	2.688	−53.923	−15,049
500,000	−150,000	−45,000	31.133	−75.436	−44,980
500,000	0	−75,000	52.354	−82.023	−74,950
500,000	150,000	−105,000	−31.284	75.676	−104,558
500,000	300,000	−135,000	−2.904	54.267	−134,695

Figure 9. The motion errors before and after compensation. (a) The position errors and (b) the orientation errors.

Table 3, and the results are shown in Figure 9(a) and 9(b), as well as the arc trajectory.

The results show the position errors of the function line along a line-trajectory and the errors of the function point along a point-trajectory are decreased enormously with compensation, while the remained errors are mainly caused by the kinematic pair errors, the repetitive position errors and the deformations caused by loads. The orientation errors of the function line cannot be compensated by the robot, as the axes and guidelines of the SCARA robot are nearly parallel. For a SCARA robot, it is infeasible to change the orientation of the function line with the driving parameters of the actual kinematic pairs, and the orientation errors should be limited in assembly.

Conclusions

An approach of robot kinematic calibration is developed by considering errors in the kinematic pairs and links. The unique features and contributions are summarized as follows.

(1) The fixed and moving axes of the revolute pair are identified by spherical image curve fittings and striction curve fittings of the discrete line-trajectories traced by all lines of the moving link. The trajectory traced by the moving axis has the minimal fitting errors, which are global invariants. The fixed and moving guidelines of the prismatic pair are indentified in the same way.

(2) The error motions of the identified moving axis or guideline relative to the fixed one are the kinematic pair errors, while the deviations of the fixed axis or guideline relative to the designed one are the link errors. These two errors are unrelated to the positions and orientations of the reference points and lines measured.

(3) The kinematic model of the SCARA robot is established by connecting the fixed elements and the moving elements of the kinematic pairs in sequence. The results show that the position errors of the robot generated by the link errors are enormously reduced by kinematic calibration, while the orientation errors should be limited in assembly.

In this work, the kinematic calibration of the robot is discussed with the kinematic invariants. The spherical image curve errors and the striction curve errors, as well as the fixed and moving axes or guidelines are all global invariants. This provides some new indexes for accuracy evaluation, and may improve the accuracy and efficiency of kinematic calibration for the industrial robots.

ORCID iD

Zhi Wang http://orcid.org/0000-0002-5007-2876

References

1. Nubiola A and Bonev IA. Absolute robot calibration with a single telescoping ballbar. *Precis Eng* 2014; 38: 472–480.
2. Nubiola A and Bonev IA. Absolute calibration of an ABB IRB 1600 robot using a laser tracker. *Robot Comput-Integr Manuf* 2013; 29: 236–245.
3. Nof SY. *Handbook of industrial robotics*. New York, NY: John Wiley, 1999.
4. Elatta A, Gen LP, Zhi FL, et al. An overview of robot calibration. *Inform Technol J* 2004; 3: 74–78.
5. Du G, Zhang P and Li D. Online robot calibration based on hybrid sensors using Kalman filters. *Robot Comput-Integr Manuf* 2015; 31: 91–100.
6. Marie S, Courteille E and Maurine P. Elasto-geometrical modeling and calibration of robot manipulators: application to machining and forming applications. *Mech Mach Theory* 2013; 69: 13–43.
7. Santolaria J, Brosed FJ, Velázquez J, et al. Self-alignment of on-board measurement sensors for robot kinematic calibration. *Precis Eng* 2013; 37: 699–710.
8. Santolaria J and Ginés M. Uncertainty estimation in robot kinematic calibration. *Robot Comput-Integr Manuf* 2013; 29: 370–384.
9. Klimchik A, Pashkevich A, Chablat D, et al. Compliance error compensation technique for parallel robots composed of non-perfect serial chains. *Robot Comput-Integr Manuf* 2013; 29: 385–393.
10. Denavit J. A kinematic notation for lower-pair mechanisms based on matrices. *J Appl Mech-Trans ASME* 1955; 22: 215–221.
11. Hayati S and Mirmirani M. Improving the absolute positioning accuracy of robot manipulators. *J Robot Syst* 1985; 2: 397–413.
12. Stone HW and Sanderson AC. Statistical performance evaluation of the S-model arm signature identification technique. In: *IEEE international conference on robotics and automation. Proc IEEE* 1988: 2: 939–946.
13. Kazerounian K and Qian GZ. Kinematic calibration of robotic manipulators. *J Mech Des* 1989; 111: 482–487.
14. Zhuang H, Roth ZS and Hamano F. A complete and parametrically continuous kinematic model for robot manipulators. *IEEE Trans Robot Autom* 1992; 8: 451–463.
15. Meng Y and Zhuang H. Autonomous robot calibration using vision technology. *Robot Comput-Integr Manuf* 2007; 23: 436–446.
16. He R, Zhao Y, Yang S, et al. Kinematic-parameter identification for serial-robot calibration based on POE formula. *IEEE Trans Robot Autom* 2010; 26: 411–423.
17. Yang X, Wu L, Li J, et al. A minimal kinematic model for serial robot calibration using POE formula. *Robot Comput-Integr Manuf* 2014; 30: 326–334.
18. Okamura K and Park FC. Kinematic calibration using the product of exponentials formula. *Robotica* 1996; 14: 415–421.
19. Chen I, Yang G, Tan CT, et al. Local POE model for robot kinematic calibration. *Mech Mach Theory* 2001; 36: 1215–1239.
20. Wu Y, Klimchik A, Caro S, et al. Geometric calibration of industrial robots using enhanced partial pose measurements and design of experiments. *Robot Comput-Integr Manuf* 2015; 35: 151–168.
21. Messay T, Ordóñez R and Marcil E. Computationally efficient and robust kinematic calibration methodologies and their application to industrial robots. *Robot Comput-Integr Manuf* 2016; 37: 33–48.
22. Abderrahim M, Khamis A, Garrido S, et al. Accuracy and calibration issues of industrial manipulators. In: LK Huat (ed.) *Industrial Robotics: Programming, Simulation and Applications*. InTech. 2006, pp.817–829.
23. Nubiola A, Slamani M and Bonev IA. A new method for measuring a large set of poses with a single telescoping ballbar. *Precis Eng* 2013; 37: 451–460.
24. Meng Y and Zhuang H. Self-calibration of camera-equipped robot manipulators. *Int J Robot Res* 2001; 20: 909–921.
25. Jang JH, Kim SH and Kwak YK. Calibration of geometric and non-geometric errors of an industrial robot. *Robotica* 2001; 19: 311–321.
26. Abderrahim M and Whittaker AR. Kinematic model identification of industrial manipulators. *Robot Comput-Integr Manuf* 2000; 16: 1–8.
27. Khalil W. Geometric calibration of robots with flexible joints and links. *J Intell Robot Syst* 2002; 34: 357–379.
28. Beyer L and Wulfsberg J. Practical robot calibration with ROSY. *Robotica* 2004; 22: 505–512.
29. Albert N, Mohamed S, Ahmed J, et al. Comparison of two calibration methods for a small industrial robot based on an optical CMM and a laser tracker. *Robotica* 2014; 32: 447–466.
30. Rauf A, Pervez A and Ryu J. Experimental results on kinematic calibration of parallel manipulators using a partial pose measurement device. *IEEE Trans Robot* 2006; 22: 379–384.
31. Joubair A and Bonev IA. Non-kinematic calibration of a six-axis serial robot using planar constraints. *Precis Eng* 2015; 40: 325–333.
32. Meggiolaro MA and Dubowsky S. An analytical method to eliminate the redundant parameters in robot calibration. In: *IEEE international conference on robotics and automation. Proc ICRA IEEE* 2000; 4: 3609–3615.
33. Rauf A and Ryu J. Fully autonomous calibration of parallel manipulators by imposing position constraint. In: *IEEE international conference on robotics and automation. Proc IEEE* 2001; 3: 2389–2394.
34. Joubair A and Bonev IA. Kinematic calibration of a six-axis serial robot using distance and sphere constraints. *Int J Adv Manuf Tech* 2015; 77: 515–523.
35. Mooring B, Driels M and Roth Z. *Fundamentals of manipulator calibration*. New York: John Wiley, 1991.
36. Rao CR, Toutenburg H, Shalabh, et al. *Linear models and generalizations: least squares and alternatives*. New York: Springer, 2008.
37. Fletcher R. *Practical methods of optimization*. Hoboken, NJ: John Wiley, 2013.
38. Omodei A, Legnani G and Adamini R. Three methodologies for the calibration of industrial manipulators: experimental results on a SCARA robot. *J Robotic Syst* 2000; 17: 291–307.

39. Shang WW and Cong S. Optimal calibration and identification of a 2-DOF parallel manipulator with redundant actuation. *Int J Robot Automat* 2015; 30: 333–344.

40. Ziegert J and Datseris P. Robot calibration using local pose measurements. *Int J Robot Autom* 1990; 5: 68–76.

41. ASME B89.3.4-2010. *Axes of rotation: methods for specifying and testing*. New York: American National Standards Institute, 2010.

42. Wang D, Wang Z, Wu Y, et al. Invariant errors of discrete motion constrained by actual kinematic pairs. *Mech Mach Theory* 2018; 119: 74–90.

43. Wang D and Wang W. *Kinematic differential geometry and saddle synthesis of linkages*. Singapore: John Wiley, 2015.

44. Wang Z, Wang D, Wu Y, et al. Error calibration of controlled rotary pairs in five-axis machining centers based on the mechanism model and kinematic invariants. *Int J Mach Tool Manuf* 2017; 120: 1–11.

45. Wu Y, Wang D, Wang Z, et al. The kinematic invariants in testing error motion of machine tool linear axes. *Mechanism and machine science: proceedings of ASIAN MMS 2016 & CCMMS 2016*. Singapore: Springer, 2017, pp.1525–1540.

Appendix 1. The displacements of the end link generated by the kinematic pairs.

	Positions	x_B/mm	y_B/mm	z_B/mm	α_B/°	β_B/°	γ_B/°
R_1	1	−1599.222	−95.936	617.273	−147.889	−0.015	−0.256
	2	−1473.651	−23.6370	617.214	−137.898	−0.011	−0.268
	3	−1325.461	−352.993	617.114	−127.892	−0.008	−0.276
	4	−1159.408	−442.033	616.984	−117.898	0.003	−0.279
	5	−980.252	−500.935	616.853	−107.892	0.008	−0.283
	6	−793.685	−527.806	616.710	−97.893	0.016	−0.285
	7	−605.172	−521.855	616.557	−87.879	0.025	−0.286
	8	−420.670	−483.267	616.420	−77.884	0.030	−0.288
	9	−245.665	−413.228	616.281	−67.887	0.037	−0.287
	10	−85.402	−313.807	616.148	−57.875	0.043	−0.285
	11	55.071	−188.135	616.019	−47.876	0.051	−0.285
R_2	1	−1541.377	506.245	617.631	−198.291	−0.037	−0.181
	2	−1562.685	218.401	617.645	−178.300	−0.040	−0.203
	3	−1484.267	−59.608	617.513	−158.328	−0.015	−0.211
	4	−1315.416	−293.975	617.377	−138.297	−0.028	−0.247
	5	−1076.617	−456.458	617.133	−118.274	−0.050	−0.312
	6	−796.793	−527.423	616.721	−98.298	0.018	−0.278
	7	−509.419	−498.424	616.314	−78.295	0.045	−0.288
	8	−249.331	−372.903	615.868	−58.293	0.076	−0.280
	9	−47.841	−165.984	615.488	−38.287	0.102	−0.265
	10	70.713	97.350	615.265	−18.285	0.121	−0.234
	11	92.030	385.374	615.223	1.712	0.132	−0.200
P_3	1	−796.617	−527.468	616.750	−171.543	3.09×10^{-4}	$−4.93 \times 10^{-3}$
	2	−796.635	−527.452	601.768	−171.542	2.78×10^{-4}	$−4.98 \times 10^{-3}$
	3	−796.665	−527.436	586.753	−171.541	3.04×10^{-4}	$−4.97 \times 10^{-3}$
	4	−796.665	−527.417	571.752	−171.540	3.19×10^{-4}	$−4.95 \times 10^{-3}$
	5	−796.726	−527.401	556.726	−171.549	3.75×10^{-4}	$−4.96 \times 10^{-3}$
	6	−796.729	−527.382	541.729	−171.544	3.39×10^{-4}	$−5.00 \times 10^{-3}$
	7	−796.746	−527.366	526.709	−171.543	3.79×10^{-4}	$−5.02 \times 10^{-3}$
	8	−796.786	−527.342	511.701	−171.548	4.08×10^{-4}	$−5.03 \times 10^{-3}$
	9	−796.808	−527.319	496.690	−171.547	4.37×10^{-4}	$−5.02 \times 10^{-3}$
	10	−796.824	−527.300	481.672	−171.545	4.69×10^{-4}	$−5.04 \times 10^{-3}$
	11	−796.844	−527.274	466.647	−171.545	5.39×10^{-4}	$−4.91 \times 10^{-3}$
R_4	1	−1167.277	−152.773	617.655	−0.238	−0.095	−173.233
	2	−1138.572	−262.085	617.524	−0.261	−0.082	−158.237
	3	−1082.621	−360.166	617.360	−0.278	−0.061	−143.260
	4	−1003.175	−440.512	617.160	−0.284	−0.037	−128.275
	5	−905.626	−497.593	616.945	−0.289	−0.008	−113.277
	6	−796.655	−527.465	616.753	−0.285	0.016	−98.291
	7	−683.580	−528.126	616.570	−0.272	0.041	−83.291
	8	−574.218	−499.516	616.426	−0.254	0.059	−68.294
	9	−475.932	−443.545	616.315	−0.231	0.076	−53.288
	10	−395.480	−364.032	616.259	−0.208	0.084	−38.284
	11	−338.349	−266.414	616.268	−0.184	0.083	−23.276